In-Pipe Rheology and Mixing Characterisation using Electrical Resistance Sensing

Machin, Thomas D.; (kent) Wei, Hsin-yu; Greenwood, Richard W.; Simmons, Mark J.h.

[Link to publication on Research at Birmingham portal](#)

In-Pipe Rheology and Mixing Characterisation using Electrical Resistance Sensing

Thomas D. Machin[a,b], Hsin-Yu (Kent) Wei[b], and Richard W. Greenwood[a], Mark J.H. Simmons[a]

[a] School of Chemical Engineering, University of Birmingham, Edgbaston, B15 2TT
[b] Industrial Tomography Systems PLC, Manchester, M3 3JZ

Abstract

This paper presents a novel, in-line Electrical Resistance Rheometry (ERR) technique which is able to obtain rheological information on process fluids, in-situ, based on electrical resistance sensing. By cross-correlating fluctuations of computed conductivity pixels across and along a pipe, using non-invasive microelectrical tomography sensors, rheometric data is obtained through the direct measurement of the radial velocity profile. A range of simple, Newtonian and non-Newtonian fluids, have been examined with the obtained velocity profiles independently validated using Particle Image Velocimetry (PIV); results from both ERR and PIV techniques are in excellent agreement. Comparison of the rheological parameters obtained from ERR with off-line rheology measurements demonstrated that ERR was able to perform with an accuracy of 98 % for both Newtonian and non-Newtonian fluids. The ERR technique presented offers new capabilities of true in-situ analysis of fluids relevant to formulated products and in-pipe spatial and temporal analyses afford the simultaneous interrogation of localised and global mixing behaviour.

Keywords: in-line, rheology, non-Newtonian, mixing, Electrical Resistance Tomography

1. Introduction

The rheological properties of a fluid system are critical in chemical and physical processing, since they govern both in-process efficiency and final product quality. Conventionally, the measurement of such properties is conducted off-line with careful sampling and removal from the product stream. The fluid rheology obtained from off-line rheometry is often considered, with assumptions, as applicable to flows in real processes. However, this approach is in the majority unsatisfactory since off-line measurements afford a retrospective characterisation of the sample structure which may not be representative of structure as a function of the time-shear history received during processing. In-situ measurements overcome this deficiency as they are inherently conducted within the flow environment and remove the possibility of degradation of the sample. Since in-line rheometer measurements are conducted within the process flow environment, they possess the capability to elevate rheometry from a quality control tool at process end-point to one which is able to control and optimise processes. Rides et al (2011) suggested in-line techniques may also afford opportunities for new product development.

There is thus an ever-increasing demand for the development of in-line rheometers as the majority of industrial complex fluids exhibit non-Newtonian behaviour. Complex fluids may observe wall slip, thixotropy, shear-induced phase migration and shear banding during processing; interpretation via conventional rheology measurements is often demanding and complex (Olmsted, 2008). Such phenomena may be captured with localised rheological measurements, with velocity profiling being a preferred technique (Ovarlez et al, 2011). The low shear rate range of in-line rheometers, 0.05 - 100 s^{-1}, is typically relevant for the rheological phenomena observed in complex systems. Despite

this, no such commercially viable technique has been outlined which is capable of performing this task efficiently across a wide range of fluids (Rees, 2014).

Aligned with this demand, numerous studies have been conducted which aim to uncover in-line rheological properties with a particular focus upon ultrasound Doppler-based velocity profiling (UVP) techniques (Wiklund et al, 2007), (Rahman et al, 2015). Despite some positive results, UVP is only applicable to systems which contain particles which act as tracers or to the velocity measurement of dispersed phase in a two-phase system (Dong et al, 2016). As a result, the applications of this technique are limited with several setups additionally prone to several sources of correlated and uncorrelated noise (Wiklund et al, 2007). Moreover, UVP cannot be applied successfully in aerated systems, greatly limiting its in-plant applicability.

Blythe et al (2017) recently implemented a Bayesian approach to pulsed field gradient Nuclear Magnetic Resonance (NMR), in one dimension, to derive in-line rheological parameters. The rheological characteristics of Carbopol 940 have been successfully extracted, demonstrating a high repeatability; however, the measured parameters do not entirely agree with conventional techniques. This study was performed with a coil tuned to a frequency of 85.2 MHz and a 2 T superconducting magnet and resultantly poses safety and economic issues, is complex and hence unlikely to be adopted within industry. Low-field NMR techniques overcome these concerns; however, the effective application of this technique to rheometry is as yet unreported. Further attempts have been made to extract the velocity profile within a pipe employing laser Doppler anemometry (Meissner, 1983) and Doppler optical coherence tomography, which are unable to interrogate opaque fluids and the latter is only currently applicable at the micro-scale (Haavisto et al, 2015).

Ren et al (2017) utilised the conductivity response of shampoo to an alteration in shear rate to extract the velocity profile without the requirement of a tracer. Electrical Resistance Tomography (ERT) was employed to measure the conductivity of each tomogram pixel; these pixels were subsequently assigned to a value of shear rate and accordingly a velocity profile was determined. Despite the removal of a tracer, the aforementioned conductivity and shear rate relationship was not defined comprehensively, requiring extensive fitting assumptions to the extent that the ERT conductivity is no longer reflective the outputted velocity profile and demonstrates poor repeatability. Shampoo additionally exhibits a comparatively large conductivity response from a minor alteration in temperature in relation to that brought about by a change in shear rate; this provides additional uncertainty (Ren et al, 2017). The aforementioned shear rate response is also unknown for a number of fluids and therefore this limits the general applicability of this technique.

The technique of electrical resistance sensing, however, still remains an extremely robust, non-invasive technique which is used to interrogate processes fluids without the limitation of optical opacity. This is derived from Electrical Impedance Tomography (EIT) which non-invasively exploits the distribution of electrical impedance to uncover information about the nature and distribution of materials located within the selected process domain (Dyakowski and Jaworkoski, 2003). The first EIT system, or Electrical Resistance Tomography (ERT) as known in process tomography, utilised in a process application was introduced by Williams et al (1995) which demonstrated dynamic interfaces of colloidal suspensions. Electrical Tomography utilises the injection of an alternating current into electrodes located at the periphery of a process vessel, or pipework, and subsequently measures the

returned voltage at the remaining electrodes, according to a pre-defined measurement protocol (Wang, 2015). These measurements are able to then be reconstructed into an image of the cross-sectional impedance distribution, known as a tomogram, to afford the visualisation and quantification of phenomena such as mixing. The wide-ranging applicability and simple implementation of microelectrical tomography sensors to industrial processing affords an ideal basis for the development of an in-line rheometer. The application of such sensors to in-pipe rheometry is termed Electrical Resistance Rheometry (ERR).

Rheologically complex fluids can also be considered to contain numerous heterogeneously mixed components with the meso- and macroscopic mixing scales playing a key role in determining the sophisticated properties of the fluid (Abadi, 2016). Extensive literature exists concerning the application of ERT to monitoring of non-Newtonian fluid mixing with imaging performed within chemical reactors (Vilar et al, 2008; Bolton et al, 2004), mixers (Pakzad et al, 2008; Carletti et al, 2014), separators and industrial pipelines (White et al, 2001; Giguère et al, 2008; Hennigson et al, 2006), the latter being the focus of this study. With the interrogation of the cross-sectional impedance map, ERR possesses the capability able to simultaneously elucidate such mixing behaviour alongside outputting parameters which monitor localised and global mixing performance.

An Electrical Resistance Rheometer has been developed which is capable of extracting the velocity profile in symmetric, laminar pipe flow; this paper outlines the methodology of this technique together with experimental measurements demonstrating its suitability for such a measurement. The chosen setup does not require the physical incorporation of tracer particles into the flow which may provide disturbances to both the product stream or contaminate the product and hence is highly advantageous over the majority of the techniques previously outlined in the literature. The capability for ERR to simultaneously extract both in-pipe rheology and local and global mixing parameters has additionally been demonstrated. Thus, ERR is able to combine two significant engineering quality and control concepts of rheology and mixing to understand inhomogeneity and non-uniformity within a process to form a powerful process characterisation tool.

2. Development of the Electrical Resistance Rheometry (ERR) Concept
2.1 Electrical Resistance Velocimetry
Electrical Resistance Rheometry (ERR) enables the in-line characterisation of a fluid's rheological behaviour via the direct measurement of the radial velocity profile and thus to elucidate the shear rate profile within a pipe. To attain this profile, a cross-correlation algorithm has been implemented to monitor the fluctuations in computed conductivity pixels of a reconstructed tomogram, see Eq. 1; this permits the tagging of fluid motion across and within multiple measurement planes, or arrays (Papoulis, 1962). As the distance between the measurement arrays is fixed and known, the extracted time delay may simply be converted to velocity.

$$R_{12}(\tau)= \int_{-\infty}^{\infty} f(t)g(t-\tau)dt \qquad (1)$$

where R_{12} is the cross correlation function; τ is the displacement between the two continuous functions, in seconds and $f(t)$ and $g(t)$ are continuous conductivity functions as a function of time.

ERR possesses a much greater temporal resolution than rotational rheometry with an acquisition time of 30 seconds which enables the monitoring of dynamic processes. This temporal resolution is a

reduction of almost 100 % when compared to NMR techniques (Blythe et al, 2017) and is also able to be further improved with the cross-correlation algorithm implemented continuously to meet the real time criterion (Kapinchev, 2015).

Sharifi and Young (2013) attempted to utilise a step change in concentration of a saline solution to tag the motion of across two planes, also known as arrays, of circular ERT sensors using AIMFLOW software, developed by Industrial Tomography Systems, ITS (ITS, 2016); however, the acquired velocity measurements do not capture the velocity profile effectively due to a lack of sensitivity in the pipe-wall boundary region. To ensure a complete velocity profile is attained, a novel, in-line ERR sensor configuration was developed which consists of a combination of electrical resistance sensor types, linear and circular arrays. The addition of linear arrays enables the specific targeting of electrical sensitivity to a desired region of interest, in this instance near to the wall. The manipulation of the linear array length, and consequently electrical field penetration, has been utilised for the first time in this study; this provides an opportunity for the development of a number of electrical resistance sensing techniques.

The sensor design of the Electrical Resistance Rheometer utilises four arrays of eight electrodes, consisting of two linear arrays and two other arrays in a circular configuration resulting in the output of four tomograms. This novel arrangement is operated using the ITS v5r system which is capable to operate a sensor consisting of a maximum of 32 electrodes; the arrays are made up of 8 electrodes as to provide the greatest temporal resolution of the v5r system and ultimately sensitivity to velocity. Linear array measurements are reconstructed to rectangular tomograms which comprise of 10 x 20 pixels and a circular tomogram consisting of 316 pixels; example tomograms produced from these sensor types are displayed above the ERR sensor in Figure 1. The inclusion of such circular sensors additionally permits the visualisation of the cross-sectional impedance map to simultaneously interrogate localised and global mixing behaviour in-line. This enables parameters such as heterogeneity index, plane-to-plane mixing index and mixing times including 95 % and 99 % mixing times.
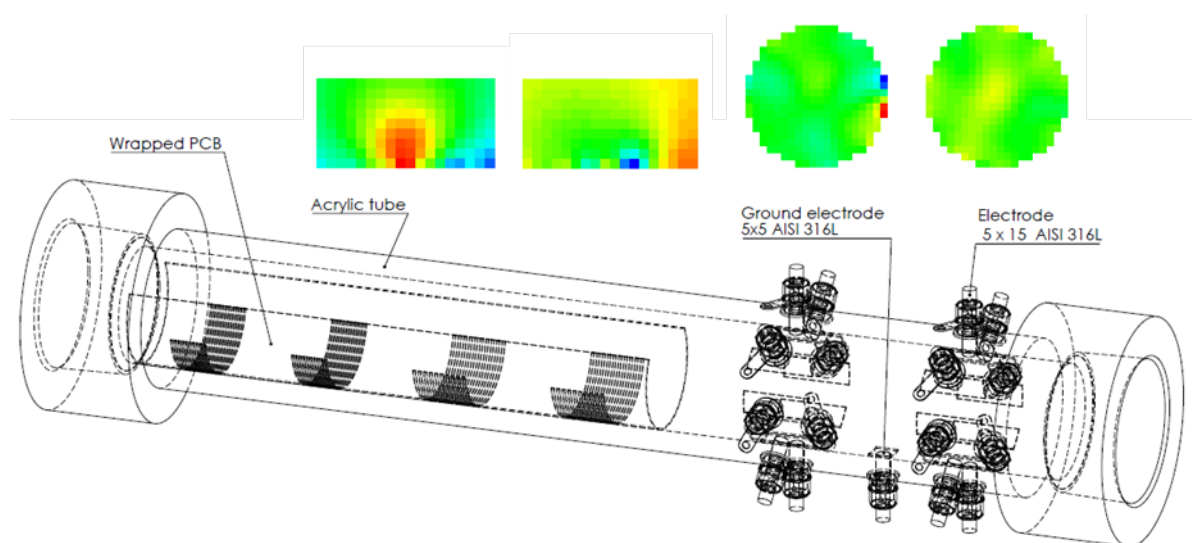

Figure 1 The Electrical Resistance Rheometry sensor design with accompanying computed tomograms

The aforementioned tomograms may be segmented into zones of interest to develop a number of radial velocity measurement positions in the pipe cross-section; the zone schemes for the aforementioned tomogram types are depicted in Figure 2. To remove noise, the bottom layer of the linear, or multi-scale, tomogram has been removed alongside the first and last three pixels, in the direction of flow, to yield nine radial velocity measurements. These nine measurements may then been further reduced to four, with pixel layer 1 of Figure 2a removed and two pixel layers averaged to just one. This alteration was implemented to introduce an 'effective' weighting to the fitting, described later in section, with a greater number of measurement points located in the central region of the velocity profile which pertain to the low shear rate region 2.2, whilst ensuring a complete velocity profile is obtained. When experimenting upon complex fluids, which observe wall phenomena, the entire zone scheme displayed in Figure 2a can be utilised to provide enhanced detail of the velocity profile near the wall. In a similar manner, the circular tomogram has been segregated with eight zones selected based upon radial position. For each of these zones, the obtained conductivity is averaged and normalised and afterwards the cross-correlation algorithm is performed across and within measurement arrays.
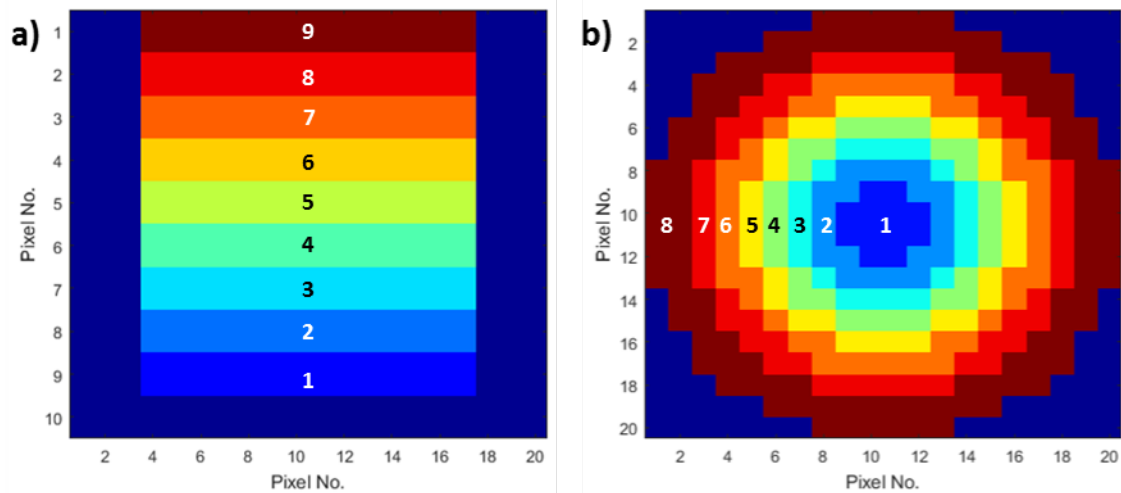

Figure 2 Tomogram Zone Scheme: (a) Linear (Multi-scale) Tomogram; (b) Circular Tomogram

For this application, a pulsed ohmic heater (C-Tech Innovation, UK) was developed to act as the required conductivity perturbation as it delivers a small increase in temperature over a short time period. This operates by imparting an alternating current, of frequency 50 Hz – 100 kHz, and hence electrical energy, to the fluid which is rapidly converted to thermal energy (Knirsch et al, 2010). An example of the produced signal, for a pixel in zone 1 in each circular array is exhibited in Figure 3a. Due to the requirement of a relatively conductive media, the range of conductivities of the test media is identical to those suitable for electrical resistance sensing, 1-30 mS cm^{-1}. Moreover, ohmic heating is advantageous as it provides uniform heating of the pipe cross-section; is 95 % efficient; has the capability for automation; does not require the physical inclusion of a tracer and minimal degradation of thermosensitive products. This extent of degradation is further limited with a required temperature rise for the ERR sensor to perform its function of only 0.7°C for 0.5 s. It is also assumed that a negligible impact upon flow properties is brought about by the affecting conductive heat dissipation; this may be quantified by the thermal Péclet number, defined as the ratio of the advective and diffusive heat transport rates and is described by Eq. 8 (Paul et al, 2004).

$$Pe = \frac{\bar{u} \cdot D_p}{\alpha} \tag{8}$$

where Pe represents the Péclet Number, $\bar{u}$ is the average flow velocity, in m s^{-1}, D_p is the pipe diameter, in m, and α is the thermal diffusivity in m^2 s$^{-1.}$

The thermodynamic and physical properties used within Eqs. 8 and 9 were extracted, from Yaws (2003), for both glycerol and water with the thermal Péclet numbers computed. However, such properties are unavailable for the aqueous xanthan gum and Carbopol solutions. As the majority of these solutions consist of water, their thermal diffusivity was estimated assuming the Stokes-Einstein relationship, where thermal diffusivity is inversely proportional to viscosity. Values of Pe thus calculated in these experiments exceeded 18 000 throughout, thus the assumption of negligible thermal diffusivity (Pe > 200) is easily justified.

Ohmic heating has extensively been applied within the food industry and as a result this robust conductivity perturbation technique is able to be operated under hygienic conditions, with rheology a critical quality control parameter in the optimisation, processing methodology and the development of many products within this industry (Maloney and Harrison, 2016). The employment of this ohmic heater develops a repeatable conductivity perturbation as depicted in Figure 3a. The subsequent implementation of the cross-correlation algorithm yields both two and three-dimensional velocity profiles. However, the velocity profile within the laminar regime is known to be axisymmetric and hence there is only a requirement for the use of the two-dimensional velocity profile in the determination of rheology (Incropera et al, 2007). To reduce computational requirements and achieve the desired high temporal resolution, ERR extracts the two-dimensional velocity profile.
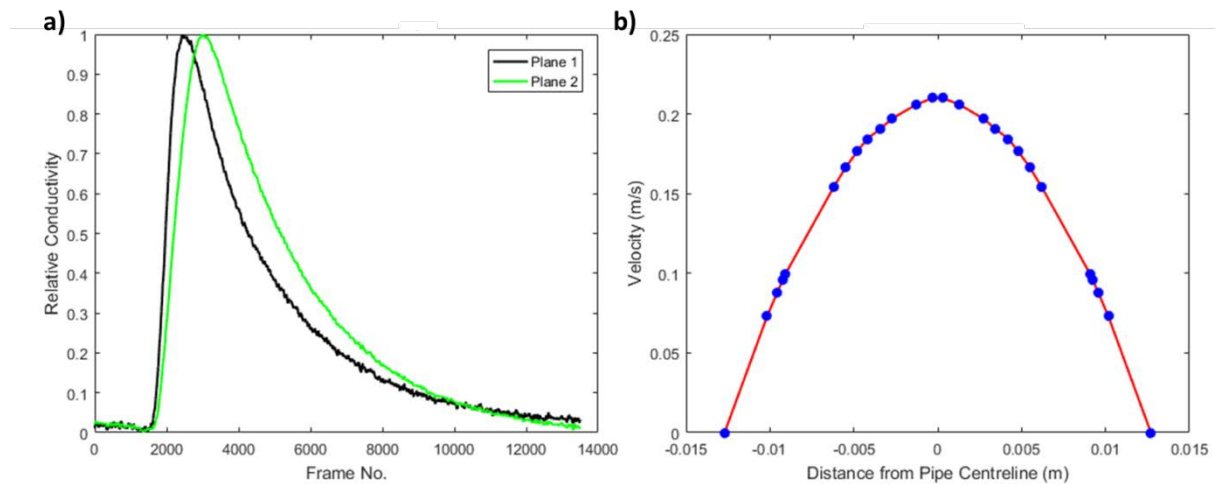
Figure 3 Electrical Resistance Rheometry sensor measurement: (a) normalised ohmic heater conductivity perturbation; (b) 75 wt% glycerol two-dimensional velocity profile

2.2 Rheology Extraction

The rheological properties of a fluid strongly influence the shape of the velocity profiles in laminar pipe flow due to a shear rate response of the fluid. Consequently, the raw velocity measurements may alone act as a fingerprinting tool; this can be utilised to infer rheological behaviour exhibited by complex fluids systems i.e. shear-banding, wall depletion and shear-induced phase migration. However, if the rheological behaviour is known to adhere to conventional rheological models, the

velocity profile shape can be related to the constitutive equation of the fluid, with the desired parameters being directly outputted. The specific constitutive equation for a power law fluid is given as:

$$\tau = k\dot{\gamma}^n = k\left(-\frac{du}{dr}\right)^n \tag{2}$$

where τ is shear stress, in Pa; k is consistency index, in Pa s^n; $\dot{\gamma}$ is shear rate, in s^{-1}, n is consistency index; u is velocity within the pipe, in m s^{-1}, and r is radius, in m.

Once extracted, the velocity profile may then be coupled with the measurement of differential pressure, ΔP, per unit length, L, to obtain the linear shear stress profile in steady state, incompressible, laminar flow as derived from a force balance on an annular element in cylindrical pipe geometry (Wilkinson, 1960).

$$\tau = \frac{\Delta P \cdot r}{2L} \tag{3}$$

where ΔP is the differential pressure drop, in Pa, along a pipe length, L, in m, with r representing a pipe radius, in m.

With the substitution of Eq. 3 into Eq. 2 and subsequent re-arrangement and integration, implementing the boundary conditions of u = 0 at r = R and u = u at r = r, the laminar velocity profile, u(r) for a power law fluid is obtained.

$$u(r) = \left(\frac{\Delta P}{2kL}\right)^{\frac{1}{n}}\left(\frac{n}{n+1}\right)\left(R^{\frac{n+1}{n}} - r^{\frac{n+1}{n}}\right) \tag{4}$$

From the first boundary condition, it can be seen that the no-slip condition has been implemented as the velocity is zero at the pipe wall radius, R; however, a correction may be made to this model for the inclusion of fluids which observe a slip layer. Rahman (2013) suggested that the combination of the imaging of the cross-sectional conductivity distribution alongside the simultaneous measurement of velocity profile or rheology may be able to provide a detailed understanding of wall-slip behaviour in rheologically complex fluids.

A parametric fitting of the raw ERR data to the theoretical velocity profile of a fluid may then be applied in the extraction of the desired rheological parameters. To derive such parameters, the Levenberg-Marquadt algorithm, a robust variant of the Gauss-Newton algorithm, which solves non-linear least squares problems iteratively was employed (Marquadt, 1968). As this selected algorithm does not possess second derivatives the overall computational time is reduced affording the aforementioned high temporal resolution. This algorithm has been utilised previously within ERT experiments; however, acting as a reconstruction algorithm (Tan et al, 2011).

The analysis may additionally be performed without the assumption of a rheological model and no prior knowledge of the material. A point-wise rheological characterisation is performed by the fitting of a 4th order polynomial to the velocity profile to obtain the velocity profile as a function of radius.

A fourth order polynomial was selected as it is the greatest fitting order without the equation becoming badly conditioned. The first derivative of this polynomial equation directly yields the shear rate profile with the shear stress profile calculated using the aforementioned differential pressure measurement. A shear stress against shear rate plot is able to be attained; this output is analogous to that of a rotational rheometer with the desired rheological parameters extracted able to be determined in the same manner as traditional rheometry. Such an approach offers a limited shear rate range, with high shear rates unreliable as a result of averaging effects near the pipe-wall (Norton et al, 2010).

2.3 Residence Time Distribution

An additional application of this sensor is the in-line measurement of the residence time distribution (RTD) within the pipe. The pulse generated from the ohmic heater may be likened to the input delta function of an RTD measurement, as a result of uniform cross-sectional heating. The continuous conductivity ERR pulse representative of the RTD response, or E-curve, which can subsequently be fitted to an appropriate mixing model such as a stirred tanks in series or axial dispersion model. From the acquisition of the velocity profile, it has been observed that the thermal diffusivity and heat loss is insignificant, due to the relatively short distance travelled and hence this technique may be considered applicable for RTD measurements.

3. Methodology

3.1 Materials

Three model aqueous-based fluids were selected to exhibit behaviour of three common rheological constitutive models, namely solutions of: glycerol (Darrant Chemicals, UK); xanthan gum, *from Xanthomonas Campestris* (Sigma-Aldrich, UK) and Carbopol 940 (Lubrizol, UK).

The formulated test fluids consisted of the mixing of 75 wt%, 85 wt% and 92.5 wt% glycerol in water and dissolving 0.1 wt%, 0.5 wt% and 1.0 wt% xanthan gum powder in water to form 15 L of aqueous solutions which exhibit Newtonian and shear thinning power law behaviour, respectively. Two Carbopol formulations were selected for this study, 0.1 wt% Carbopol, pH 7 and 1.0 wt% Carbopol, pH 7 as these are known to act as a rheological mimetic for an industrial fluid (Simmons et al, 2009). The pH of the aqueous Carbopol solutions was adjusted with the incorporation of 0.1 M Sodium Hydroxide, supplied by Sigma-Aldrich, to induce a gel matrix whose rheological behaviour may be described using the Herschel-Bulkley constitutive law (Alberini et al, 2014). The mixing of all fluids was carried out slowly to prevent the incorporation of air bubbles. A portable conductivity meter, supplied by Hanna Instruments was utilised to determine the electrical conductivity of the fluids. All of the experimental fluids observe an electrical conductivity within the range of 1-9 mS cm^{-1} and hence are suitable for ERR.

The rheological properties of the fluids were analysed using an AG R2 rotational rheometer (TA Instruments) equipped with a smooth-walled, 4.006° stainless steel cone and plate geometry of diameter 40 mm. The sample was held at 23 ± 0.1°C using an Peltier plate, before a logarithmic shear rate ramp was applied across the shear rate range of 0.01 - 1500 s^{-1}, over a duration of 600 seconds with 20 points per decade. The selected temperature was chosen as it is reflective of the temperature of the fluid in the subsequent flow experiments. To analyse the obtained data, a non-

linear least squares regression was applied in the TRIOS software, developed by TA instruments, to extract fitted rheological parameters; this analysis is similar to that utilised in the ERR analysis to elucidate rheological parameters. Such a fitting was performed at the low shear rate range, 0.01-100 s^{-1}, which is analogous to shear rates observed in pipe flow and removes errors which may occur due to weighting of the velocity profile. This low shear rate region is often the area of greatest interest when extracting more complex rheological behaviour. The resultant rheological properties acquired are presented in Table 2, Section 4.3.

3.2 Electrical Resistance Tomography

A simple recirculating pipeline was setup, Figure 4, which consisted of an agitated 60 L vessel and a controlled positive displacement pump (Fristam Ltd., UK) operated by a personal computer to circulate the fluid at a desired flow rate. The electrical resistance rheometer sensor, of diameter 25.4 cm, was placed in-line, with the ohmic heater located prior to the ERR sensor in series. The measurement of differential pressure was captured across the length of both the ohmic heater and ERR sensor and logged alongside the parameters of flow rate and temperature. The flow rate was monitored using a micro motion Coriolis flow meter (Emerson Ltd., UK).
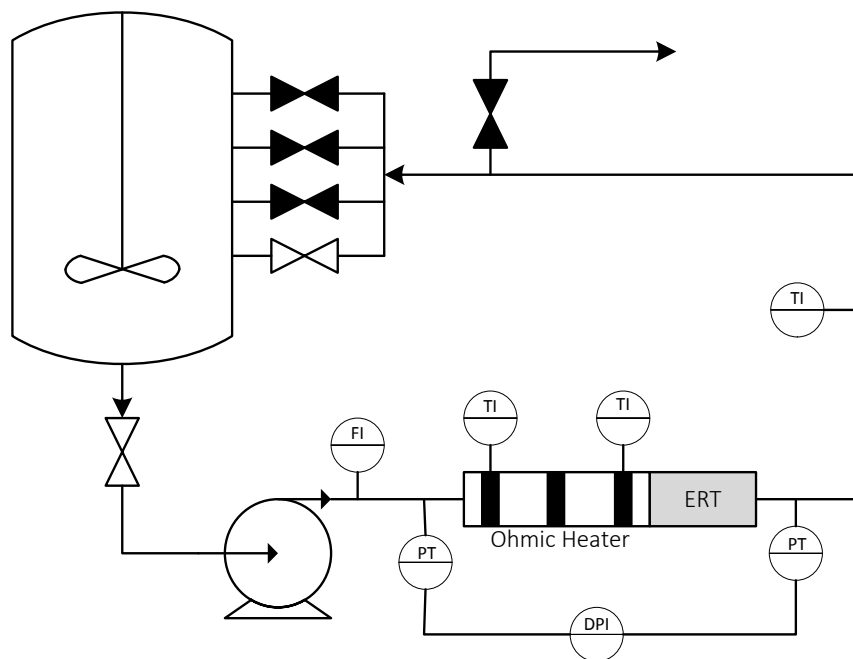
Figure 4 Experimental flow loop setup schematic

Each of the fluids were interrogated across the flow rate range of 40 – 350 L hr^{-1}, with the ERR sensor connected to and operated by a v5r ERT instrument (Industrial Tomography Systems (ITS) Ltd., UK). A configuration of 4 planes, or arrays, of 8 electrodes was utilised alongside the adjacent electrode measurement protocol. The sensor was operated with two linear arrays, of length 12 mm, and two circular arrays employed. To enable a frame rate of 325 frames per second, the v5r was operated in block mode and one sample delay cycle. For a single measurement 12 000 (37 seconds) frames were taken to monitor the desired conductivity perturbation generated by the ohmic heater,

whose voltage injection was set in the range of 1 − 1.5 kV for 0.5 − 1 s. The entire experimental procedure was repeated 20 times at each flow rate for each fluid to assess repeatability.

The obtained raw data was fed into a MATLAB code which contained the Modified Standard Back projection algorithm (Wang, 2002), this was utilised to reconstruct the tomogram image, and the subsequent rheological analysis, described in Section 2.2. Supplementary experiments were undertaken to determine the capability of simultaneous capture of both rheological and mixing behaviour. This was conducted using 15 L of aqueous 0.1 wt% xanthan gum solution with a step change in xanthan gum concentration brought about with the addition of a 3.5 wt% solution; the resultant batch volume and concentration was 17 L and 0.5 wt%, respectively. The xanthan gum powder in the concentrated solution was mostly, but not entirely, dissolved as to interrogate more variable mixing phenomena with some polysaccharide agglomerates present. Across 25 minutes, the rheological properties and mixing times of the recirculating fluid were examined using a code developed in MATLAB; the ITS p2+ V8 software was employed to investigate mixing behaviour in a more thorough manner.

3.3 Particle Image Velocimetry (PIV)

Validation of the cross-sectional velocity profile has been provided by 2-D PIV measurements which were achieved using a TSI PIV system. A 532 nm (green) laser (Litron Nano PIV), pulsed at 7 Hz, is synchronised to a single TSI Power view 4MP (2048 x 2048 pixels) 12 bit CCD camera using a synchroniser (TSI 610035) assigned to a personal computer. The TSI Insight 4G software was utilised to control the software, process data and generate velocity fields with subsequent radial velocity profile measurement averaging performed in MATLAB. The Nyquist PIV algorithm, developed by TSI, was used to obtain such velocity fields; this setup is analogous to the one used by Alberini et al (2017) but has been adapted to monitor pipe flow.

PIV measurements were conducted within a circulation loop without the inclusion of the ohmic heater to determine the extent of its effect upon the measured velocity profile. For each of the assigned flow rates, 500 images were captured, erroneous data removed, and the remaining data combined with average flow field determined. The erroneous data occurred as a result of vibration of the rig perpendicular to the flow direction between pulses; this occurred on an average of 10 frames per 500 captures, however, is not problematic due to the laminar nature of the flow. The spatial resolution of such a setup, supplied by TSI Inc, was 12 μm pixel[-1] with an interrogation area set to 64 x 64 pixels and the Gaussian peak method applied to identify single particles (Westerweel, 1997). All of test fluids were experimented upon with the exception of 1.0 wt% xanthan gum due to its opaque nature.

4. Results and Discussion
4.1 Electrical Resistance Velocimetry
4.1.1 In-Pipe Velocity Profiling

Critical to the in-situ determination of rheology, the measurement of the velocity profile must first be interrogated with the obtained results for each fluid outlined in Figure 5.
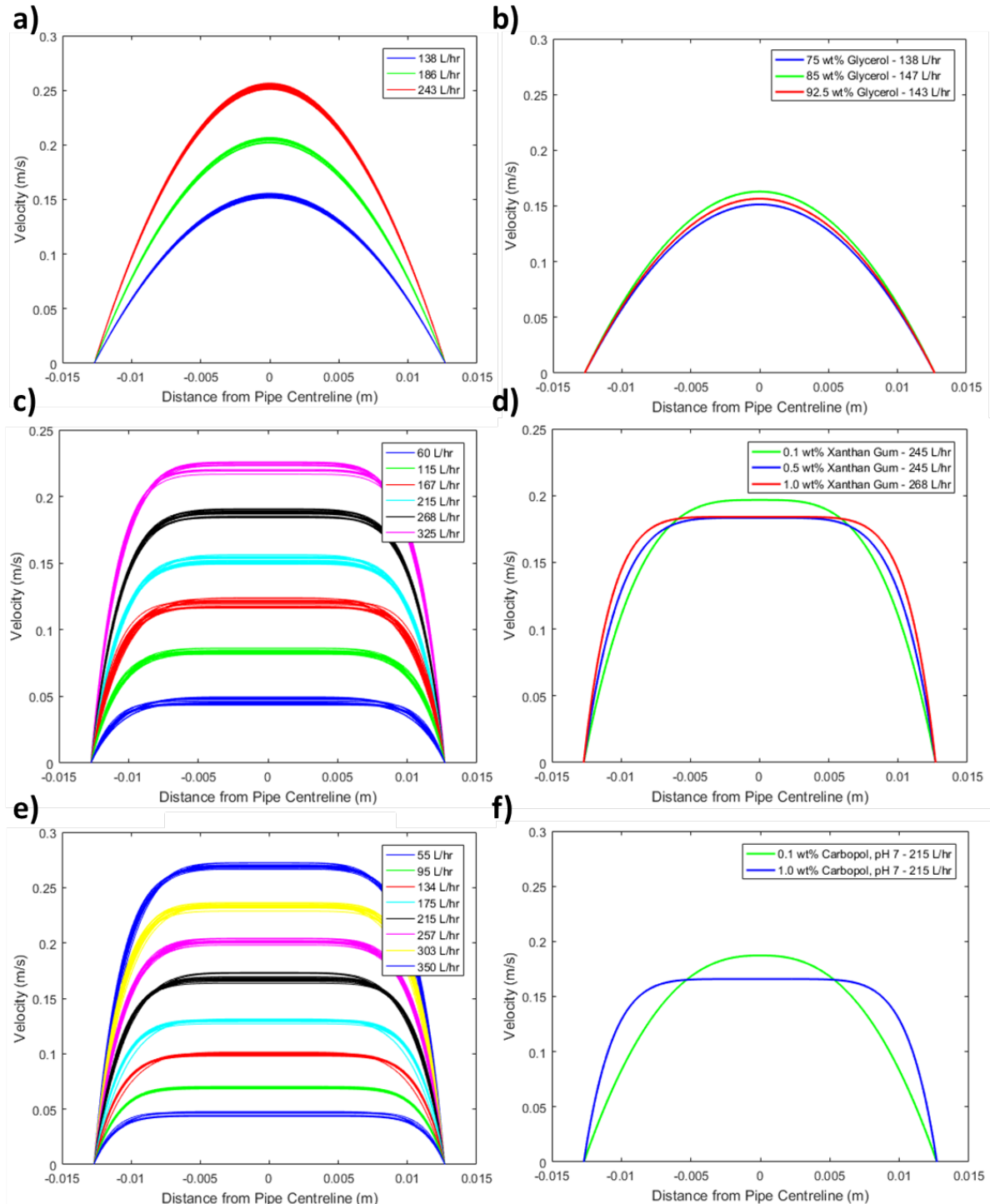
Figure 5 Electrical Resistance Rheometry Velocity Profiles: (a) 75 wt% glycerol – multiple flow rates; (b) averaged velocity profiles for 75, 85, 92.5 wt% glycerol at similar flow rates; (c) 1.0 wt% xanthan gum – multiple flow rates; (d) averaged velocity profiles for 0.1, 0.5 and 1.0 wt% xanthan gum at similar flow rates; (e) 1.0 wt% Carbopol, pH 7 – multiple flow rates; (f) averaged velocity profiles for 0.1 wt%, pH7 and 1.0 wt%, pH 7 Carbopol 940 at similar flow rates

The velocity profiles within this figure are acquired from the cross-correlation of a single conductivity perturbation passing through the sensor; these perturbations typically have a duration of 20 seconds From the obtained velocity profiles, it is evident that the Newtonian glycerol solutions observe the conventional parabolic velocity profile of laminar pipe flow, which is reflected in both fitted profiles,

11

Levenberg-Marquadt, Figures 5a and 5b, and gradient-based techniques and raw data. Such a parabolic shape implies that hydrodynamic entrance effects have apparently been overcome in this measurement allowing the application of laminar flow theory to rheological extraction to be successful. Not only is the parabolic shape in agreement with the theoretical laminar velocity profile, but the maximum velocity mirrors that expected from the measured flow rates.

When changing the fluid to the shear-thinning, xanthan gum solutions, the difference in shear rate response yields the expected increased blunting of the originally parabolic velocity profile with increased xanthan gum content. This flattening of the velocity profile is indicative of the expected shear-thinning behaviour and is illustrated in Figure 5c. During experimentation, unfortunately, an identical flow rate was unable to be attained when measuring 0.5 wt% and 1.0 wt% xanthan gum and hence a perfect comparison is not able to be conducted. However, in Figure 5d, it can still be seen that for a 1.0 wt% xanthan gum solution the obtained velocity profile observes increased flattening, and hence degree of shear-thinning, in comparison to the aqueous, 0.5 wt% xanthan gum solution, despite the former conducted at a greater flow rate.

A similar shape is observed during the extraction of the Herschel-Bulkley modelled Carbopol 940 solutions, Figure 5e, with this region instead indicative of a plug flow and thus the presence of a yield stress. As the flow rate increases, the radius of such a plug is reduced signifying that the yield stress is being tracked; this is due to the increased magnitude of the opposing shear stress profile at an increased flow rate. Initially, it can be seen that the features of the outputted velocity profiles are in accordance expected theoretical velocity profiles. Moreover, a comparison of the two Carbopol concentrations observes a large difference in the length of the plug region of the velocity profiles which is indicative of the higher yield stress of the more concentrated 1.0 wt%, pH Carbopol solution. It could therefore be stipulated that the velocity profiles mimic the theoretical velocity profiles of the fluids which have been tested upon and demonstrate repeatability throughout with minor variations of the velocity profile observed at a constant flow rate.

To quantify such promising results, a statistical analysis has been performed across 20 independent ERR velocity profiles for each discrete radial velocity position; this yields an average 95 % confidence interval of ± 2.93 % when compared to the mean. This variation manifests as a mean standard error in velocity of just 0.0043 m s^{-1} which is seen to be consistent across all radial positions. Resultantly, measurement points located near the wall observe a greater uncertainty; however, this is dampened in the overall fitting due to an 'effective' weighting with more discrete radial velocity measurement at the centre of the pipe. This is also an important factor when determining rheological parameters, with the region of interest typically the low shear rate region which coincides with the velocity at the centre of the pipe. The radial velocity profile obtained by ERR may be considered to be in close agreement with the theoretical laminar velocity profile with a typical correlation coefficient, R^2, of 0.99 between raw and accepted velocity values which additionally lie within one standard error of one another.

4.1.2 Coriolis Flow Meter Validation

The use of a positive displacement pump for this test gives rise to potential pulsation within the flow with a variation in flow rate, Q, logged using the Coriolis flow meter, of ± 2 %. This is analogous to the outputted data by Electrical Resistance Rheometry and hence the measured velocity profiles can

be said to lie within experimental error. The presence of this flow meter within the flow loop provides a further basis for comparison against an independent and established measurement technique. Using the general relationship, Eq. 5, derived from flow through an annular element of radius r and width dr, the acquired velocity profile can subsequently be utilised to determine the flow rate within the pipe.

$$Q = \frac{\pi R^3}{\tau_w^3} \int_0^{\tau_w} \tau^2 f(\tau) \, d\tau \tag{5}$$

where Q is volumetric flow rate, in $m^3 \, s^{-1}$; R is pipe radius, in m; τ is shear stress profile, in Pa, and τ_w is the shear stress at the wall which is defined by Eq. 3 with r equal to the pipe radius.

A parity plot, Figure 6, may be used to compare the obtained flow rates from a Coriolis Flow meter and Electrical Resistance Rheometry with excellent agreement, yielding a correlation coefficient of 0.9956. Despite observing a greater variability, ERR produces a mean standard error of $\pm 6 \, L \, hr^{-1}$ and consequently may be considered repeatable. This affords validation of the ERR technique with an independent measurement technique which is well-established.
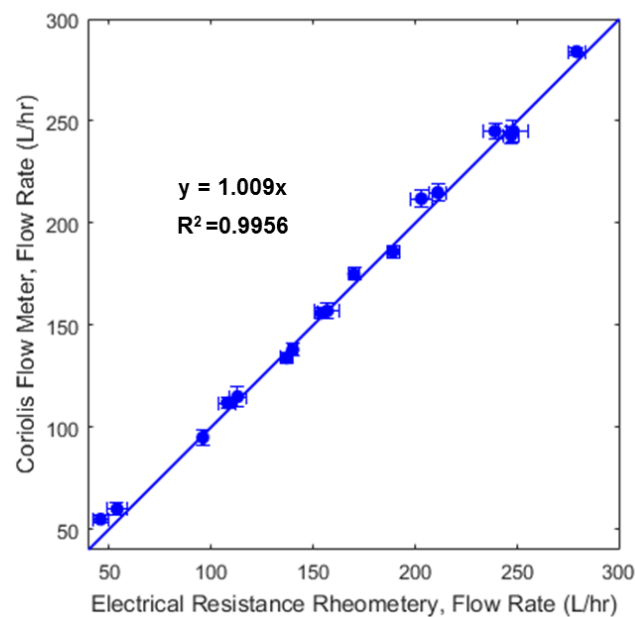

Figure 6 A parity plot comparing the measured flow rate from a Coriolis Flow Meter and Electrical Resistance Rheometry

4.1.3 Velocity Profile Analysis (No Prior Knowledge)
As outlined in Section 2.2, an alternative velocity profiling methodology, gradient-based, may be applied to the fitting, which does not require prior knowledge of the fluids rheological behaviour. Subsequently, this may be compared with the Levenberg-Marquadt fitted velocity profile with a resultant correlation coefficient of 0.997 for aqueous glycerol solutions. Such a high correlation indicates that the extent of the parametric fitting is minimal and hence the raw data is an accurate representation of the velocity profile. With an increased blunting of the velocity profile, the degree of correlation is reduced to 99.0 %, 98.0 %, 97.3 % and 96.1 % for aqueous solutions of 0.5 wt%

13

xanthan gum, 1.0 wt% xanthan gum, 0.1 wt% Carbopol 940 and 1.0 wt% Carbopol 940, respectively. This occurs due to the existence of localised maximum and minima in the polynomial fitting in the flat region of the velocity profile. Consequently, it is recommended that the gradient-based methods are not applied to fluids which exhibit high levels of 'apparent' shear-thinning behaviour; this is in agreement with Wiklund et al (2010).

However, in such cases the raw velocity profile data points alone may be utilised as a rheological fingerprinting tool, especially when considering more complex rheological phenomena that do not adhere to conventional models.

4.2 Particle Image Velocimetry

Despite providing a valuable comparison, the Coriolis flow meter does not provide a direct validation of the measured velocity profile shape and magnitude. However, the application of Particle Image Velocimetry (PIV) allows Electrical Resistance Rheometry to be quantifiably validated against a widely accepted and extensively studied velocimetry technique of superior spatial resolution. The obtained results from 75 wt% glycerol at a flow rate of 240 L hr^{-1} are displayed in Figure 7b and 7c alongside an example capture, Figure 7a, with the anticipated parabolic velocity profile observed.

Comparing ERR with the theoretical Newtonian velocity profile, the PIV measurement possesses a residual sum of squares of 4.43×10^{-4} m^2 s^{-2} and a correlation coefficient of 0.9992 and accordingly, the Glycerol velocity profile can truly be considered parabolic. This provides a vital result as irrotational flow region has been achieved due to the removal of hydrodynamic entrance effects, which permits the application of traditional laminar flow theory. This region ensures that the laminar hydrodynamic boundary layer has encompassed the entire pipe diameter and prevents the flattening of the traditional velocity profile (Incropera et al, 2007).

$$L_{lam} = 0.05 \cdot Re \cdot D_p \tag{6}$$

where L_{lam} is the laminar entrance length, in m; Re is Reynolds number and D_p is the pipe diameter, in m.

The 75 wt% glycerol solution additionally yields the largest Reynolds number, and hence hydrodynamic entrance length, of 20 cm, due to its relatively low viscosity and high density. This is in agreement with the experimental design since the circular sensor arrays, which monitor the central pipe region, are located 41 cm from the closest potential flow disturbance, the live ohmic heater electrode. Therefore, the assumptions of fully developed laminar flow is no longer an assumption affording laminar flow theory and specific constitutive rheological models to be applied, during the rheology extraction, across all of the interrogated fluids. Moreover, the flow field can be seen to be axisymmetric; this is an additional assumption which has been made during the rheological determination which may now be removed.

Not only does the parabolic nature remove assumptions, both the shape and magnitude of the radially averaged velocity mimic the velocity profiles obtained by electrical resistance sensing. The velocity vectors are all present in the axial direction of flow with a negligible radial velocity component; this is also indicative of traditional laminar theory. When the observed velocity outside

the diameter is excluded, a correlation coefficient, R^2, of 0.99 exists between the ERR and PIV glycerol velocity profiles with a root mean squared error (RMSE) of just 0.0064 m s^{-1} which is representative of 3.7 % of the average velocity. Therefore, the independent velocity profile measurements displaying excellent agreement for the Newtonian glycerol solution.
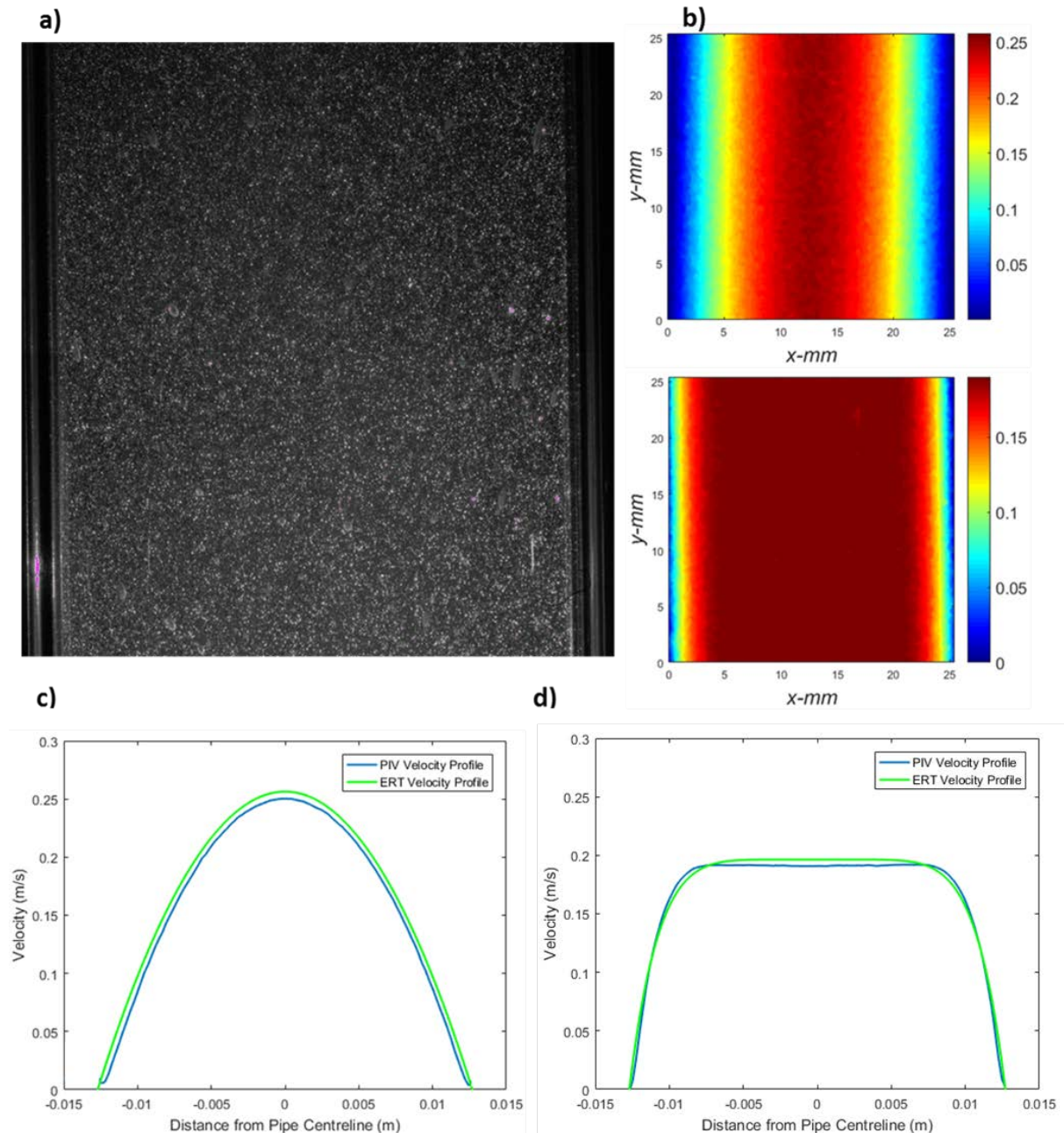

Figure 7 PIV Cross-Sectional Velocity Profile: (a) example PIV capture for this setup; (b) PIV velocity magnitude output for glycerol at 240 L hr^{-1} (top) and 1.0 wt% Carbopol 940, pH 7 at 260 L hr^{-1} (bottom); (c) comparison of the radially averaged PIV glycerol velocity profile and average ERR velocity profile; (d) comparison of the radially averaged PIV Carbopol velocity profile and average ERR velocity profile

This is also true when the rheology of the process media is changed. The aforementioned blunted velocity profile characteristic of the yield stress fluid, 1.0 wt% Carbopol, pH 7, is obtained in both the PIV and ERR measurements. A similar comparison as conducted for glycerol may be performed with an outputted RMSE of 0.0048 m s^{-1}, 2.8 % of the average velocity, and correlation coefficient of 0.99.

Despite this experiment being conducted without the presence of the ohmic heater, the acquired velocity profiles obtained from both PIV and ERR are analogous. Thus, it may be stipulated that the thermal energy dissipation has a negligible impact upon the flow. The similarity between the comprehensive PIV measurement, theoretical laminar velocity profiles and Electrical Resistance Tomography is a significant validation of this novel in-line velocity profile measurement technique.

The obtained velocity profile may therefore be utilised unaccompanied as a fingerprinting in-line rheometer, especially in the case of more rheologically complex fluids which do not adhere to specific constitutive models and equations. This study has also verified the electrical field penetration of the linear arrays velocity vectors, within the conductivity range of 1-9 mS cm^{-1}. It must be noted that the radial velocity positions remained constant throughout all experiments and is expected that this electrical field penetration is also applicable to fluids of conductivity in excess of 10 mS cm^{-1}.

4.3 Rheological Parameter Extraction

The rheological parameters determined by ERR are compared to off-line rotational rheometry in Table 1. In the measurement of accuracy, the rheological parameters outputted by the rotational rheometer may be considered as the 'true' value; however, it is known that a direct comparison of the two rheometry techniques is imperfect as ERR affords a characterisation within the flow environment. It must be noted the experimental data acquired by the AR G2 rotational rheometer was performed once, with only one sample taken and hence may not be entirely reflective of the product stream.

Using ERR, the mean obtained viscosities for 75 wt%, 85 wt% and 92.5 wt% glycerol solutions were 0.0223 Pa s, 0.0982 Pa s and 0.250 Pa s, respectively. With the requirement of just a single parameter to be extracted, the viscosity of a Newtonian fluid is able to be achieved with excellent reliability with the 95 % confidence interval approximately 2.5 % of the mean value. This may be observed in Figures 8b and 8c which observe minimal difference between the rotational rheometer and ERR. Despite being small, this variation in viscosity is seen to portray a relationship between the experimental temperatures of the fluid experiment with the inverse proportionality temperature and viscosity observed. The rheological behaviour of glycerol is known to be highly thermosensitive (Chen and Pearlstein, 1987). In addition to such repeatability, the measured viscosity displays good agreement with the accepted technique within industrial processing, a rotational rheometer with an average accuracy of 99.1 %. Therefore, the rheological parameters obtained by off-line rheometers is analogous to that of ERR in the same case of simple fluids; this may differ depending on the complexity of the fluid and off-line experimental protocol. However, it can be said that this technique is able to act as an in-line viscometer.
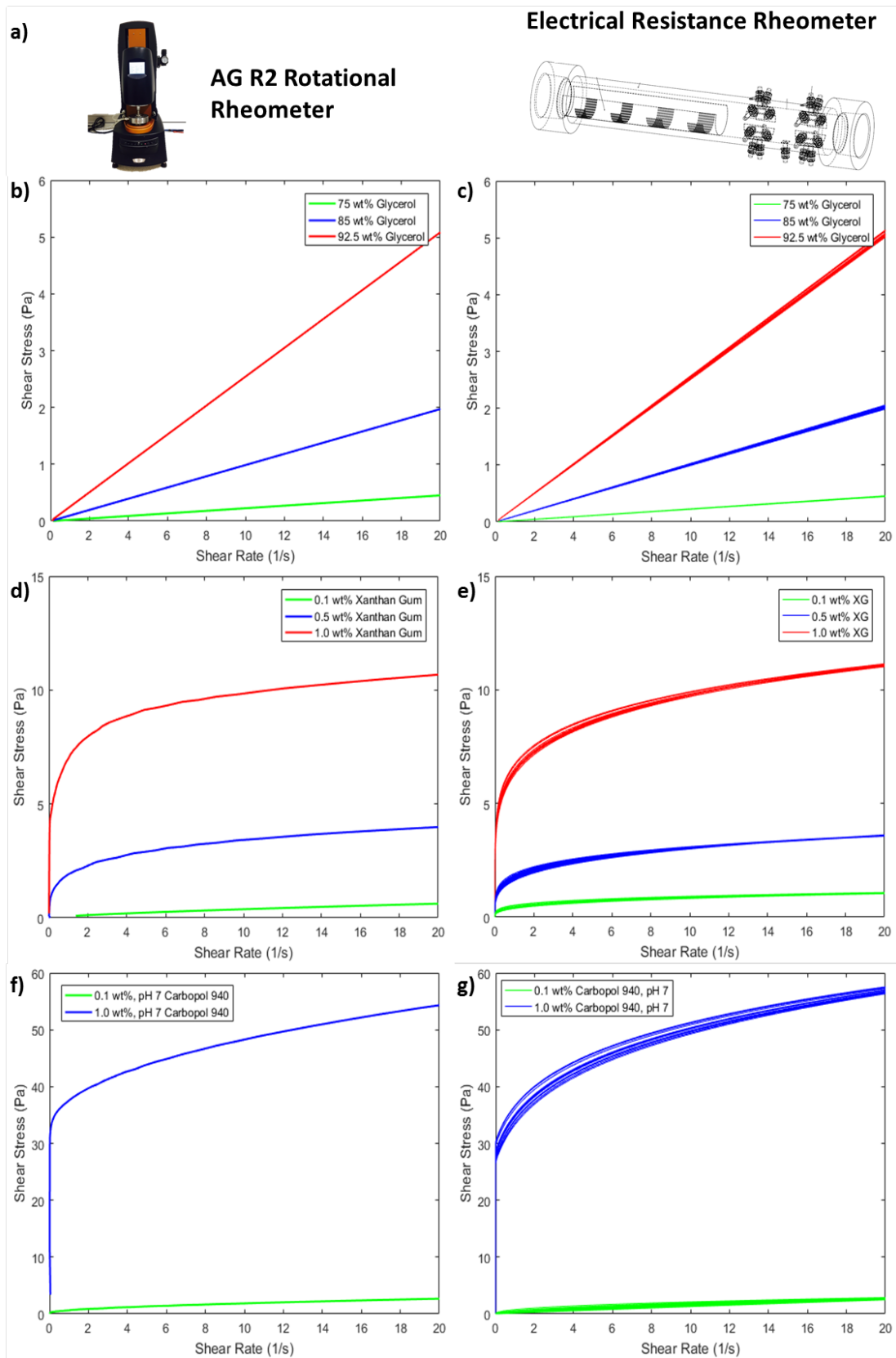
Figure 8 Comparison of ERR and rotational rheometry: a) Images of the rotation and ERR rheometer; b), d) and f) shear stress vs. shear rate plot generated from a rotational rheometer for glycerol, xanthan gum and Carbopol, respectively; c), e) and g) shear stress vs. shear rate plot generated for glycerol, xanthan gum and Carbopol using an Electrical Resistance Rheometer, respectively

As the complexity of the selected constitutive model increases, a simple univariate model validation is not adequate. The parameter estimation becomes an ill-conditioned mathematical problem; the constitutive models may be described by two or more parameters with the analysis performed from a single velocity profile. Owing to the ill-conditioned nature of this mathematical problem, the parametric fitting of this model against a single objective function does not validate entire model and does not support model outputs (Stitt et al, 2015). A measure of the residual squares alone, R^2, can be said to be an inadequate criterion in the analysis of a parametric fitting with the mathematical form of equations able to contribute to an apparent 'good' fit. However, the adjustable parameters of the fitting can be poorly predicted with the least squares alone an unreliable indicator of quality of model fit or model discrimination. Stitt et al (2015) reported that in nineteen reaction kinetics models fitted to the same datasets with R^2 values in excess of 95 %, many exceeding 99 %, were observed.

Although the inadequacies of the residuals squares analysis alone are evident, this technique has been traditionally utilised across all rheometry. In the analysis of ERR, the evaluation of the quality of fit has been extended to the statistical quality of the parameter estimates, with the common approach of 95 % confidence interval of the adjustable parameters interrogated across the 20 independent measurements. Moreover, this confidence interval possesses an inherent link between observations, noise within the data and the degrees of freedom to yield a more complete analysis of the obtained data (Sjöblom, 2009). The extracted rheological parameters are displayed in Table 1, alongside both the least squares residuals and 95 % confidence intervals.

Table 1 A comparison of an off-line rotational Rheometer with the Electrical Resistance Rheometer. Note: The uncertainty represented within this Table is the 95% confidence interval of the fitted parameters.

	TA R2 Rotational Rheometer			Electrical Resistance Rheometer		
Material	μ, Pa s			μ, Pa s		
75 wt% Glycerol	0.0226 (R^2=0.9997)			0.0223 ± 0.0004 (R^2 = 0.994)		
85 wt% Glycerol	0.0986 (R^2=0.9993)			0.0982 ± 0.003 (R^2 = 0.995)		
92.5 wt% Glycerol	0.254 (R^2=0.9993)			0.250 ± 0.004 (R^2 = 0.992)		
	τ_y, Pa	k, Pa s^n	n	τ_y, Pa	k, Pa s^n	n
0.1 wt% XG		0.0712	0.723 (R^2 = 0.99)		0.0740 ± 0.003	0.704 ± 0.04 (R^2 = 0.99)
0.5 wt% XG		1.27	0.350 (R^2 = 0.991)		1.21 ± 0.04	0.348 ± 0.02 (R^2 = 0.99)
1.0 wt% XG		6.13	0.195 (R^2 = 0.995)		6.18 ± 0.2	0.197 ± 0.01 (R^2 = 0.993)
0.1 wt% Carbopol, pH 7	0.350	0.342	0.604 (R^2 = 0.999)	0.32 ± 0.02	0.372 ± 0.02	0.601 ± 0.04 (R^2 = 0.99)
1.0 wt% Carbopol, pH 7	29.7	5.93	0.460 (R^2 = 0.991)	29.1 ± 1.7	5.80 ± 0.3	0.486 ± 0.04 (R^2 = 0.994)

The power law behaviour of xanthan gum is described by both the consistency index, k, and power index, n, and hence poses an ill-conditioned problem; however, the incorporation of the Levenberg-Marquadt algorithm has been seen to be vital to dampen the instability and increase confidence in the measurement. Contrary to this, the acquired ERR rheological parameters are seen to mimic those obtained from a conventional rotational rheometer possessing an accuracy of 97.4 % and 98.5 % for k and n, respectively. It can be seen that the fitting of the 0.1 wt% and 0.5 wt% xanthan gum

shear rate ramp represents the lowest correlation coefficient of 0.99; this is analogous to the fitting of the raw ERR velocity data to the theoretical profile.

As expected, the introduction of a third parameter through the utilisation of the Herschel-Bulkley model produces the greatest variability of the measurement at around ± 6 %. Despite the outputted rheological additionally observing reduced accuracy, when compared to a rotational rheometer, the values obtained from ERR can be seen to be in good agreement. This arises as a consequence of the parametric fitting with the off-line rheometer parameters yielding a theoretical velocity profile which has a correlation coefficient of 0.97 with the ERR velocity profile. This may be reflected as the outputted values from the off-line rheometer lie within the 95 % confidence interval of the ERR rheometry. Although Carbopol solutions are typically considered not to exhibit thixotropic properties, shear-dependent history at > 0.2 wt% concentration has been witnessed (Lubrizol, 2002) which may give rise to a difference in the obtained rheological properties. It must additionally be acknowledged that the of the 0.1 wt% Carbopol 940 solution may be modelled with a power law rheological model as a result of the presence of a small yield stress. When fitting to off-line rheometry data, 0.1 wt% Carbopol yielded a correlation coefficient of 0.999 for both power law and Herschel-Bulkley constitutive equations.

Overall, the non-linear least square fitting from the ERR accurately and repeatedly outputs the desirable rheological parameters which mimic conventional rotational rheometry. ERR can therefore be utilised as an effective, robust, in-line rheometer when the Levenberg-Marquadt algorithm is employed. However, when employing the gradient based method, instabilities may arise with numerous oscillations between local minima and maxima due to the polynomial fitting. This is in agreement with Wiklund et al (2007) who recommend that this analysis methodology should be employed for profiles which are relatively parabolic. If the fluids are not known to adhere to conventional rheological models this velocimetry technique may additionally act as a standalone fingerprinting tool for rheology without the requirement of the measurement of differential pressure.

4.4 Mixing Analysis
4.4.1 Mixing Time and Rheometry
As it provides the mapping of electrical impedance across the cross-section of the sensing domain, ERT has extensively been utilised to monitor the mixing performance across numerous unit operations. With the inclusion of a circular array within the ERR sensor design such an analysis is permitted during the simultaneous capture of rheometry. A step increase in the concentration of aqueous xanthan gum solution, as described in Section 3.2, has been successfully interrogated with the tomogram capable of providing an averaged cross-sectional conductivity within the pipe. Due to xanthan gum possessing a dissimilar conductivity to water, the averaged tomogram conductivity affords a detailed examination of mixing time. A 95 % mixing time, Θ_{95}, of 13 minutes 22 seconds and 99 % mixing time, Θ_{99}, of 20 minutes 4 seconds was ascertained for the mixing of these aqueous xanthan gum solutions; 80 %, 85 % and 90 % mixing times were also calculated. When blending in stirred tanks, the concentration differences are seen to decrease exponentially; this yields Eq. 11 (Paul et al, 2004).

$$\frac{d(1-C)}{d\theta} = -k(1-C) \qquad\qquad (11)$$

Integrating the above equation, between the boundary conditions C = 0, Θ = 0 and C = C, Θ = Θ, yields a linear relationship between the natural log of the concentration difference and mixing time; this may be utilised to predict mixing times of different extents. Figure 9c, displays such a plot with the aforementioned linear relationship observed with a gradient of -0.191 min^{-1} and residual squares of 0.9854. The reliability of the mixing time measurement is enhanced when compared with traditional mixing time calculations which utilise a single point conductivity probe; the ERR measurement is performed across two pipe regions and throughout the entire cross-section. Figure 9a, demonstrates the average tomogram pixel conductivity utilised for this mixing time computation and within this measurement exists four pulses from the ohmic heater which are utilised to simultaneously elucidate rheology.

The ERR methodology was utilised alongside the parametric Levenberg-Marquadt algorithm fitting, to output the rheology from the four aforementioned pulses. A pulse may be observed just after 30 seconds prior to the step increase in xanthan gum concentration with the computed ERR flow curve and rheological parameters mirroring those of a 0.1 wt% aqueous solution outlined in section 4.3. However, upon the addition of xanthan gum an evolution in the rheological behaviour may be observed with an apparent increase in both the consistency index and shear-thinning nature of the fluid; this is to be expected. The final rheological parameters acquired during this test, at 18 minutes and 30 seconds, are a consistency index and power index of 1.17 Pa s^{n} and 0.40, respectively; this is similar to the parameters obtained from 0.5 wt% xanthan gum rheological measurements. Such results may be observed in Figure 9b. This time may be considered the point at which the rheology is almost completely evolved which is in alignment with the measured 95 % mixing time measurement as these rheological parameters were after the 95 % mixing time.

Although, in this instance, rheometry data was collected at six minute intervals, the ERR system possesses a much greater temporal resolution with the interval time able to be reduced to 30 seconds. This evolving rheological measurement in other processes may be linked with the monitoring displacement of fluids within a pipe which can be utilised during product changeover, start-up and shutdown. Henningsson et al (2007) was able to monitor the rinsing step, in which yoghurt is displaced by water with the use of a hygienic ERT sensor system and displayed good agreement with Computational Fluid Dynamics (CFD).
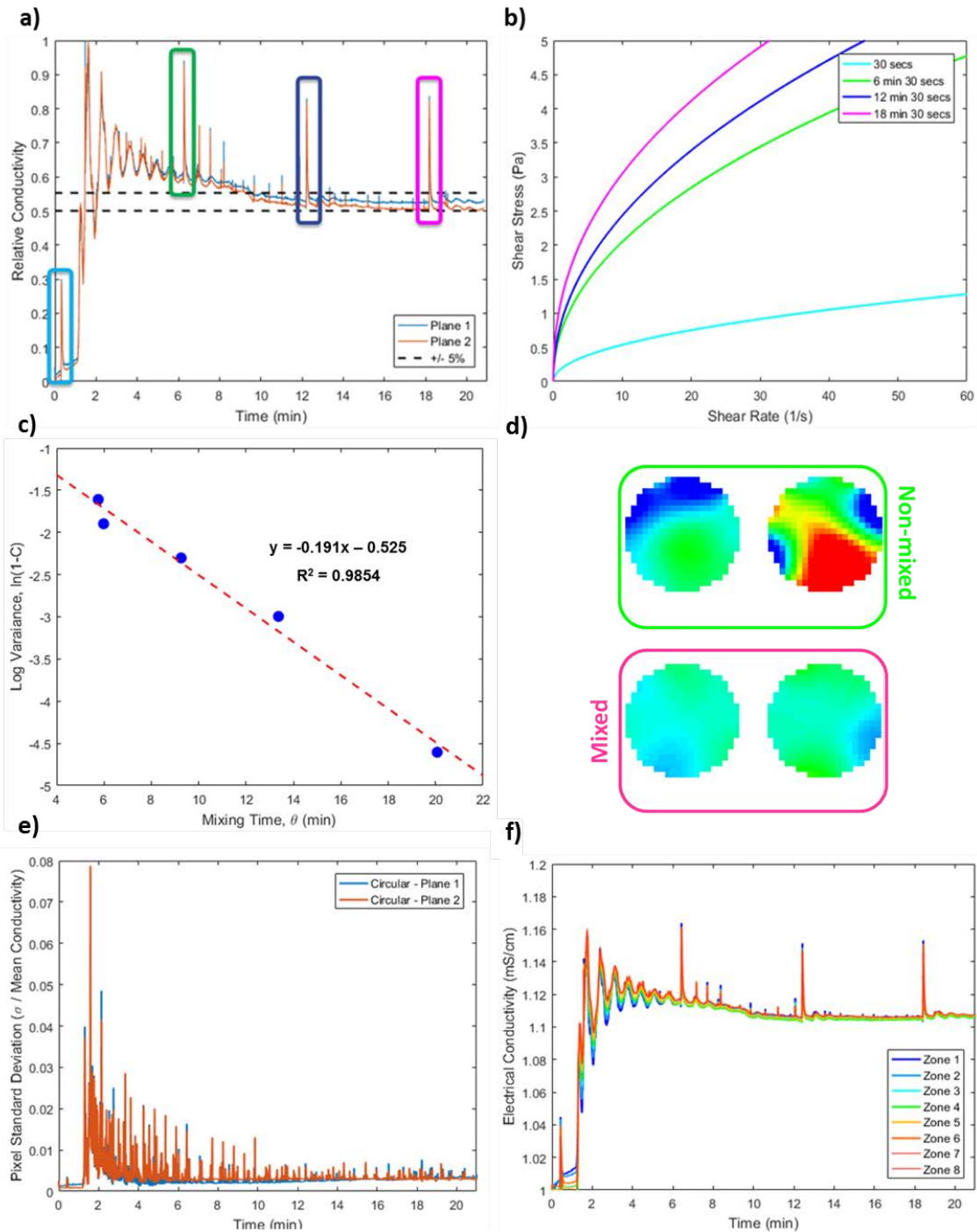
Figure 9 Step change in xanthan gum concentration with the addition of an 3.5 wt% aqueous solution to a 0.1 wt% solution: (a) relative conductivity plot with ohmic heater pulses highlighted; (b) evolving xanthan gum rheology with time; (c) plot of log variance against mixing time; (d) circular tomograms at 5 minutes (top box) and 20 minutes (bottom box); (e) tomogram pixel standard deviation with time; (f) zone average conductivity.

4.4.2 Localised Mixing

The mixing phenomena may be interrogated further with the use of the tomogram produced by the two circular arrays. Such arrays afford the visualisation, Figure 9d, of the pipe cross-section and consequently interrogate radial mixing phenomena. A timewise reduction in the more conductive polysaccharide agglomerate size until only a single phase was observed. The location of these

agglomerates was additionally able to be traced across two arrays to ensure that no build-up occurred.

The tomograms depicted in Figure 9d can then be scrutinised further on a pixel basis to determine localised mixing behaviour, with an analysis of pixel standard deviation and zoned averages able to be performed. Figure 9e, displays the standard deviation of measured conductivity across each of the 316 pixels of a circular tomogram to provide an understanding radial homogeneity within the pipe and is comparable to the global mixing parameter, coefficient of variance. A sharp rise in standard deviation is initially observed which then appears to decay exponentially until a plateau is reached; this plateau is in agreement with the mixing time relationship established previously within this section. Moreover, numerous perturbations, of decreasing magnitude, exist within this measurement which also elucidates the presence of polysaccharide agglomerate. From this figure it may additionally be concluded, that the impact of the temperature rise, and therefore conductivity change, brought about by the ohmic heater is minimal relative to the mixing phenomena and hence is not likely to impede on the analysis of mixing.

The tomogram may be segmented further to determine whether any localised mixing phenomena have occurred, with the selected zones the same as those utilised for the rheological analysis, Section 2.1, Figure 2b. Figure 9f presents the conductivity for each of these zones; however, as each of the zones observe a similar trend, minimal information is able to be extracted. It can be seen that closer to the wall, Zone 8, the presence of high concentration xanthan gum is witnessed around 20 seconds later than in Zone 1. Furthermore, it is in agreement with the pixel standard deviation described previously with the conductivity value of all zones converging to 1.113 mS cm^{-1} and hence is considered radially homogenous.

4.4.3 Residence Time Distribution

The ohmic heater pulse itself can additionally be utilised in the measurement of residence time distribution (RTD); however, this refers to the pipe alone and not the entire re-circulation setup. The ERR continuous conductivity function, Figure 3a, is representative of the conventional output RTD response, E-curve, with the typical exponential decay of the laminar profile observed. This signal, Figure 10a, may be fitted to a Newtonian laminar flow in pipes model which may be described by Eq. 12 (Levenspiel, 1999). This resulting E-curve may then be summed cumulatively to produce the cumulative RTD, or F-curve.

$$E(t) = \frac{\tau^2}{4t^3}$$

(12)

where E(t) is the mean residence time distribution, t is time, in seconds, τ is the average residence time, in seconds.

As the ohmic heater pulse is provides uniform heating across a length of 20 cm and over a time period 0.5 seconds, the conventional delta input of is not present. Accordingly, the input pulse has been calculated and subsequently applied to the laminar flow in pipes model; this outputted E-curve is pictured in Figure 10a.
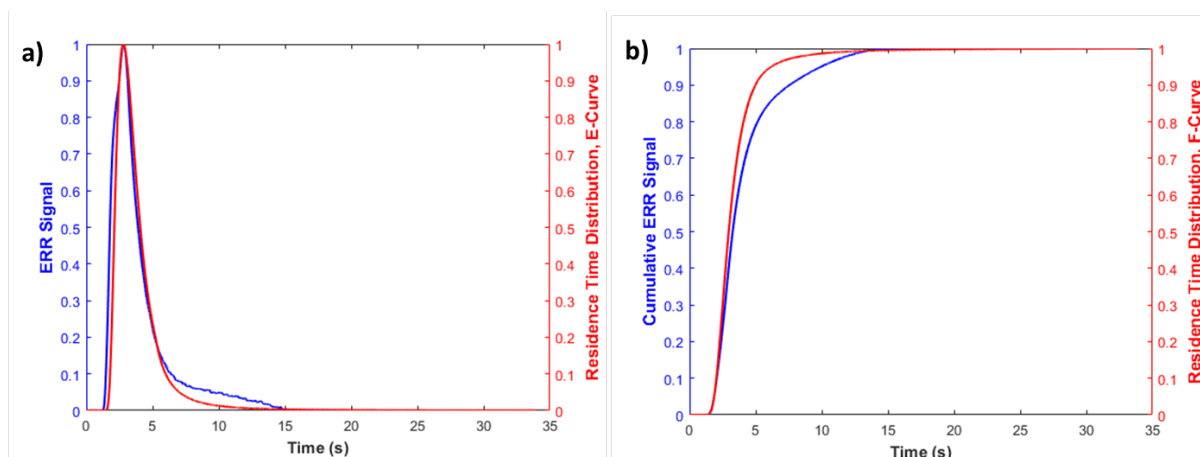
Figure 10 Comparison of the ERR and theoretical laminar flow in pipes RTD for 75 wt% glycerol at 156 L min^{-1}: a) E-curve; b) F-curve.

The outputted ERR signal and theoretical laminar E-curve can be seen to be analogous, with a correlation coefficient of 0.94. As a consequence of this similarity in the measurement domain, the conductivity, or heat, perturbation delivered by the ohmic heater may be considered as both uniform and at steady state over the applied time period. This demonstrates an additional potential of this ERR setup to be utilised in the in-line extraction of RTD when more complex flows patterns are present i.e. in the presence of a static mixer.

5. Conclusions

An Electrical Resistance Rheometry (ERR) technique has been presented which utilises a novel arrangement of non-invasive, microelectrical tomography arrays to elucidate the in-situ rheological behaviour of process fluids. This technique is advantageous over conventional off-line techniques as it is able to be directly applied to the process environment and removes the requirement for physical sampling. This in-line measurement has been achieved utilising the cross-correlation of computed conductivity pixels to tag the motion of a fluid in the pipe to extract a radial velocity profile. A novel electrical resistance sensor has been developed which consists of two electrode arrangements, linear and circular. The manipulation of the linear array length, and ultimately electrical field penetration, to target sensitivity to the near-wall region and ensure a complete velocity profile was achieved; this methodology may be employed in numerous operations for example stirred vessel.

The acquired velocity profiles were then validated using the well-established technique of Particle Image Velocimetry, which not only was in excellent agreement, but also validated the assumptions made in the rheological extraction. As the correlation coefficient between these two techniques was found to be 0.99, the electrical resistance rheometer can be said to act as a velocimetry fingerprinting tool for rheology. ERR coupled with the measurement of differential pressure was then additionally was seen to be in excellent agreement with rotational rheometry across a range of fluids described by differing constitutive behaviour. This comparison yielded an agreement of 98 % for rheological parameters of both Newtonian and non-Newtonian fluids.

Spatial and temporal analysis of the pipe cross-section additionally affords the simultaneous interrogation of mixing behaviour with extensive mixing information captured. Traditional ERT mixing analyses and parameters have been performed with mixing times, visualisation of mixing

phenomena and residence time distributions extracted. Hence, two significant formulation quality concepts were then able to be combined with the simultaneous analysis of mixing behaviour. This sensor therefore offers new capabilities of the in-situ analysis of fluids relevant to formulated products with respect to process optimisation, understanding and control.

6. Acknowledgements

7. References

1. Abadi, S. (2016). *The Role of Rheology in the Flow and Mixing of Complex Fluids.* PhD Thesis University of Birmingham: Birmingham.

2. Alberini, F; Simmons, M.J.H; Ingram, A; Stitt, E.H. (2014). Use of an areal distribution of mixing intensity to describe blending of non-Newtonian fluids in a Kenics KM static mixer using PLIF. *AIChE Journal*. 60, 332-242.

3. Alberini, F; Liu, L; E.H. Stitt, M.J.H. Simmons. (2017). Comparison between 3-D-PTV and 2-D-PIV for determination of complex fluids in a stirred vessel. *Chemical Engineering Science.* 171, 189-203.

4. Blythe, T.W; Sederman, A; Stitt, E.H; York, A; Gladden, L. (2017). PFG NMR and Bayesian Analysis to Characterise non-Newtonian Fluids. *Journal of Magnetic Resonance.* 274, 103-114.

5. Bolton, G; Hooper, C; Mann, R; Stitt, E.H. (2004). Flow distribution and velocity measurement in a radial flow fixed bed reactor using electrical resistance tomography. *Chemical Engineering Science.* 59, 1989-1997.

6. Carletti, C; Montante, G; Westerlund, T; Paglianti, A. (2014). *Analysis of solid concentration distribution in dense solid-liquid stirred tanks by electrical resistance tomography. Chemical Engineering Science.* 119, 53-64.

7. Chen, Y; Pearlstein, A. (1987). Viscosity-Temperature Correlation for Glycerol-Water solutions. University of Illinois: Chicago.

8. Dong, X; Tan, C; Dong, F. (2016). Oil-water two-phase flow measurement with combined ultrasonic transducer and electrical sensors. *Measurement Science and Technology.* 27(12).

9. Dyakowski, T; Jaworski, A. (2003). Non-Invasive Process Imaging – Principles and Applications of Industrial Process Tomography. *Chemical Engineering Technology*. 26(6), 697-706.

10. Griguere, R; Fradette, L; Mignon, D; Tanguy, P.A. (2008). Charcterization of slurry flow regime transitions by ERT. *Chemical Engineering Research and Design.* 86, 989-996.

11. Haavisto, S; Koponen, A; Salemela, J. (2015). New insight into rheology and flow properties of complex fluids with Doppler optical coherence tomography. *Frontiers in Chemistry: Fibres and Biobased Materials.*

12. Incropera, F; De Witt, D; Bergman, T.L; Lavine, A. (2007). *Fundamentals of Heat and Mass Transfer. 6th Ed.* John Wiley and Sons: New York.

13. Industrial Tomography Systems PLC (ITS). (2016). *AIMFLOW.* Available: https://www.itoms.com/products/aimflow/. Last accessed 8th Jan 201827.

14. Kapinchev, K; Bradu, A; Barnes, F; Podoleanu, A. (2015). GPU implementation of cross-correlation for image generation in real time. *IEEE Xplore.*

15. Knirsch, M; dos Santos, C; de Oliveira Soares Vicente, A; Vessoni Penna, C. (2010). Ohmic Heating, A Review. *Trends Food Sci.* 21(9), 436-441.

16. Levenspiel, O. (1999). *Chemical Reaction Engineering.* John Wiley and Sons: New York.

17. Lubrizol Advanced Materials Inc, Flow and Suspension Properties of Carbopol© Polymers, Technical Data Sheet (TDS-180). (2002). The Lubrizol Corporation: Ohio, 369-276.

18. Maloney, N; Harrison, M. (2016). *Innovation and Future Trends in Food Manufacturing and Supply Chain Technologies.* Elsevier: Amsterdam.

19. Marquadt, D. (1963). An algorithm for least squares estimation on non-linear parameters. *SIAM J App Maths.* 11, 431-444.

20. Meissner, J. (1983). Polymer Melt Flow Measurements by Laser Doppler Velocimetry. *Polymer. Test.* 3 (4), 291-301.

21. Norton, I; Spyropoulos, F; Cox, P. (2010). *Practical Food Rheology.* Wiley-Blackwell: London, 33-41.

22. Olmsted, P. (2008). Perspectives on shear banding in complex fluids. *Rheologica Acta.* 47, 283-300.

23. Ovarlez, G; Mahaut, F; Bertrand, F; Chateau, X. (2011). Flows and Heterogeneities with a vane tool: Magnetic resonance imaging measurements. *J. Rheol.* 55, 197-223.

24. Pakzad, L; Ein-Mozaffari, F; Chan, P. (2008). Using electrical resistance tomography and computational fluid dynamics modelling to study the formation of caverns in the moxing of pseudoplastic fluids possessing a yield stress. *Chemical Engineering Science.* 63, 2508-2522.

25. Papoulis, A. (1962). *The Fourier Integral and Its Applications.* McGraw-Hill: New York. 244-253.

26. Paul, E.L; Atiemo-Obeng, V; Kresta, S. (2004). *Handbook of Industrial Mixing: Science and Practice*. Wiley-Interscience: New York.

27. Rahman, M; Hakansson, U; Wiklund, J. (2015). In-line Rheological Measurements of Cement Grouts: Effects of water/cement ratio and hydration. *Tunneling and Underground Space Technology.* 45, 34-42.

28. Rahman, N. (2013). *Wall Slip in Pipe Rheometry of Multiphase Fluids.* PhD Thesis, University of Manchester: Manchester.

29. Rees, J. (2014). Towards online, continuous monitoring for rheometry of complex fluids. *Advances in Colloid and Interface Science.* 206, 294-302.

30. Ren, Z; Kowalski, A; Rodgers, T.L. (2016). *Estimating Inline Velocity Profile of Shampoo using Electrical Resistance Tomography (ERT).* 8th World Congress of Industrial Process Tomography.

31. Ren, Z; Kowalski, A; Rodgers, T. (2017). Measuring Inline Velocity Profile of Shampoo by Electrical Resistance Tomography (ERT). *Flow Measurement and Instrumentation.* 58, 31-37.

32. Rides, M; Jezek, J; Derham, B; Moore, J; Cerasloi, E; Simler, R; Perez-Ramirez. (2011). Viscosity of concentrated therapeutic protein compositions. *Advanced Drug Delivery Reviews:* 63(13), 1107-1117

33. Sharifi, M; Young, B. (2013). Electrical Resistance Tomography (ERT) for flow and velocity profile measurement of a single phase fluid in a horizontal pipe. *Chemical Engineering Research and Design:* 91 (7), 1235-1244.

34. Simmons, M.J.H; Edwards, I; Hall, J.F; Fan, X; Parker, D.J; Stitt, E.H. (2009). Techniques for Visualisation of Cavern Boundaries in Opaque Industrial Systems. *AIChE Journal*. 55(11), 2765-2772.

35. Sjöblom, J. *Parameter Estimation in Heterogeneous Catalysis.* PhD Thesis, Chalmers University of Technology: Sweden.

36. Stitt, H; Marigo, M; Wilkinson, S; Dixon, T. (2015). How Good is Your Model? *Johnson Matthey Technol. Rev.* 68(2), 74-89.

37. Tan, C; Xu, Y; Dong, F. (2011). Determining the boundary conditions of inclusions of known conductivities using a Levenberg-Marquadt algorithm by electrical resistance tomography. Meas. Sci. Technology. 22.

38. Vilar, G; Williams, R; Wang, M; Tweedie, R. (2008). On line analysis of structure of dispersions in an oscillatory baffled reactor using electrical impedance *tomography*. *Chemical Engineering Journal:* 141, p58-66.

39. Wang, M. (2002). Inverse Solutions for Electrical Impedance Tomography Based on Conjugate Gradients Methods. *Measurement Science and Technology*. 13, 101-117.

40. Wang, M. (2015). *Industrial Tomography.* Elsevier Science: Amsterdam

41. Westerweel, J. (1997). Fundamentals of digital particle image velocimetry. *Meas. Sci. Technol*. 8, 290, 294-301.

42. White, R; Simic, K; Strode, P. (2001). The Combined Use of Flow Visualisation, Electrical Resistance Tomography and Computational Fluid Dynamics Modelling to Study Mixing in a Pipe. *2nd World Congress on Industrial Process Tomography.*

43. Williams, RA; Nisbet, A; Dickin, F.J; Taylor, S. (1995). Microelectrical Tomography of Flowing Colloidal Dispersions and Dynamic Interfaces. *Biochem. Eng. J.* 56(3), 143-148.

44. Wilkinson, W.L. (1960). *Non-Newtonian Fluids – Fluid Mechanics, Mixing and Heat Transfer*. Pergamon Press Ltd: London, 1-38.

45. Wiklund, J; Shahram, I; Stading, M. (2007). Methodology for In-line Rheology by Ultrasound Doppler Velocity Profiling and Pressure Difference Techniques. *Chemical Engineering Science*. 62(1), 4277-4293.

46. Wiklund, J; Stading, M; Trägårdh, C. (2010). Monitoring liquid displacement of model and industrial fluids in pipes by in-line ultrasonic rheometry. *Journal of Food Engineering*. 99(1*), 330-337.*

47. Yaws, C. (2003). *Yaws Handbook of Thermodynamic and Physical Properties of Chemical Compounds.* Knovel. Online version available at: https://app.knovel.com/hotlink/toc/id:kpYHTPPCC4/yaws-handbook-thermodynamic/yaws-handbook-thermodynamic. Last accessed: 20/01/2018.

48. Yenjaichon, W; Grace, J; Lim, C; Bennington, C. (2013). Characterisation of gas mixing in water and pulp-suspension flow based on electrical resistance tomography. *Chemical Engineering Journal.* 214, 285-297.